Journal of Magnetic Resonance **139,** 389–401 (1999)
Article ID jmre.1999.1805, available online at http://www.idealibrary.com on IDEAL®

Determination of Multiple ϕ-Torsion Angles in Proteins by Selective and Extensive ^{13}C Labeling and Two-Dimensional Solid-State NMR

Mei Hong

Department of Chemistry, University of Massachusetts, Amherst, Massachusetts 01003

Received January 27, 1999; revised April 28, 1999

We describe an approach to efficiently determine the backbone conformation of solid proteins that utilizes selective and extensive ^{13}C labeling in conjunction with two-dimensional magic-angle-spinning NMR. The selective ^{13}C labeling approach aims to reduce line broadening and other multispin complications encountered in solid-state NMR of uniformly labeled proteins while still enhancing the sensitivity of NMR spectra. It is achieved by using specifically labeled glucose or glycerol as the sole carbon source in the protein expression medium. For amino acids synthesized in the linear part of the biosynthetic pathways, [1-^{13}C]glucose preferentially labels the ends of the side chains, while [2-^{13}C]glycerol labels the C^{α} of these residues. Amino acids produced from the citric-acid cycle are labeled in a more complex manner. Information on the secondary structure of such a labeled protein was obtained by measuring multiple backbone torsion angles ϕ simultaneously, using an isotropic–anisotropic 2D correlation technique, the HNCH experiment. Initial experiments for resonance assignment of a selectively ^{13}C labeled protein were performed using ^{15}N–^{13}C 2D correlation spectroscopy. From the time dependence of the ^{15}N–^{13}C dipolar coherence transfer, both intraresidue and interresidue connectivities can be observed, thus yielding partial sequential assignment. We demonstrate the selective ^{13}C labeling and these 2D NMR experiments on a 8.5-kDa model protein, ubiquitin. This isotope-edited NMR approach is expected to facilitate the structure determination of proteins in the solid state.

Key Words: **^{13}C labeling; proteins; torsion angle; resonance assignment; solid-state NMR.**

INTRODUCTION

Recently solid-state NMR has been increasingly applied to the structure determination of noncrystalline and disordered biological molecules. Techniques that yield both distance and orientational constraints to high precision are now available. The sensitivity of these NMR experiments is greatly enhanced by the enrichment of NMR-sensitive isotopes such as ^{13}C and ^{15}N. So far, most NMR structural studies of solid peptides and proteins have adopted a specific-labeling approach whereby a small number of sites in the molecule is labeled in each synthesis and then one or two distances or torsion angle constraints are measured in each experiment (*1–7*). To determine protein structures more efficiently and comprehensively, it is desirable to employ more extensive isotopic labeling approaches and to extract multiple structural constraints from each experiment. The second condition may be fulfilled by performing two-dimensional (2D) NMR experiments where one dimension separates and identifies the chemically distinct sites through their isotropic chemical shifts, while the other dimension yields the structural parameters (*8*). The first condition can be fulfilled by uniform ^{13}C and ^{15}N labeling of the proteins, which is used routinely now in solution NMR to determine the structure of globular proteins (*9, 10*). In solid-state NMR, uniform ^{15}N labeling has also been utilized to obtain information such as the orientation of protein segments in the membrane bilayer (*11*). However, uniform ^{13}C labeling of proteins leads to several spectroscopic difficulties for solid-state NMR. First, the one-bond ^{13}C–^{13}C *J*-couplings and the multispin dipolar couplings that are effective in fully ^{13}C-labeled proteins cause significant line broadening. The *J*-coupling-induced line broadening cannot be removed by magic-angle spinning (MAS) alone (*12, 13*) while the dipolar-induced line broadening is only removed completely at very high spinning speeds ($>$25 kHz) (*14*). Thus the spectral resolution of fully ^{13}C-labeled proteins is limited under normal MAS speeds (3–15 kHz). Second, the weak ^{13}C–^{13}C dipolar couplings that reflect long-range ^{13}C–^{13}C distances are obscured by the strong couplings between directly bonded ^{13}C spins. This occurs by spin diffusion within the dense ^{13}C spin network and by the dipolar truncation mechanism (*15, 16*). These spectroscopic challenges, combined with the high cost of ^{13}C labeling, have hindered the routine measurement of multiple structural constraints in solid proteins from a single experiment and on a single sample.

In this paper we explore selective and extensive ^{13}C labeling as a means to facilitate the NMR investigation of solid proteins and demonstrate the application of ϕ torsion measurement on such a labeled model protein, ubiquitin. By exploiting the biosynthetic pathways of amino acids in bacteria, we can incorporate ^{13}C labels into some sites in the proteins while leaving other sites unlabeled. Easily feasible with the standard protocol for protein expression, the selective and extensive (S&E) labeling approach reduces the number of directly-bonded ^{13}C spin pairs or larger clusters in the molecule, either by not labeling one of the carbons in the chain, or by reducing

1090-7807/99 $30.00

the labeling levels of the sites involved. The principal advantage of this S&E labeling approach for solid-state NMR lies in the resolution enhancement that it achieves. This is demonstrated by the ^{13}C spectra of several differently labeled ubiquitin (M_r = 8565, 76 residues). The abundant X-ray crystal diffraction (*17*) and solution-state NMR (*18–21*) data that are available for ubiquitin allow us to verify the ^{13}C labeling protocol and to demonstrate the solid-state NMR techniques. The modest molecular weight of ubiquitin also makes it possible to assess the realistic sensitivities of the NMR experiments. Similar selective ^{13}C labeling approaches have been applied in solution NMR for measuring precise relaxation parameters (*22, 23*); however, to our best knowledge this is the first demonstration of selective ^{13}C labeling for solid-state NMR investigation of protein structure.

Using a ^{13}C selectively and ^{15}N uniformly labeled ubiquitin sample, we demonstrate the residue-specific measurement of backbone torsion angles ϕ by correlating the N–H and C^{α}–H^{α} bond orientations (*24*). The ϕ-angle experiment yielded site-specific information on the backbone conformation with an accuracy of ± 5 to $\pm 30°$, by comparison with the X-ray crystal structure. Since structure determination requires the assignment of spectral resonances to the residues in the protein sequence, we applied a ^{15}N–^{13}C 2D correlation technique and demonstrate that it is possible to achieve partial sequential assignment directly in the solid state.

RESULTS AND DISCUSSION

1. Selective and Extensive ^{13}C Labeling

The selective and extensive labeling method relies on the specificity of the amino acid biosynthetic pathways in bacteria. Under aerobic conditions, bacteria can utilize glucose or glycerol as the sole carbon source to synthesize the 20 amino acids. This is achieved via three major enzymatic pathways: glycolysis, the pentose phosphate pathway, and the citric-acid cycle (*25, 26*). As an example, we outline the metabolic fates of the glucose C1 carbon in Fig. 1. During glycolysis, the six-carbon glucose is oxidized to the three-carbon pyruvate, converting glucose C1 into the pyruvate methyl carbon, C3. Since glucose C1 and C6 contribute equally and indistinguishably to pyruvate C3, only 50% of pyruvate results from glucose C1. Pyruvate is next oxidized to acetyl-CoA, which enters the citric-acid cycle, where two key intermediates, α-ketoglutarate and oxaloacetate, serve as the precursors for 10 amino acids. Oxaloacetate is also produced directly from phosphoenolpyruvate and pyruvate through several anaplerotic reactions. Both α-ketoglutarate and oxaloacetate are reused in the cyclical reactions, thus labeling multiple carbon sites, particularly C^{α}, C^{β}, and C^{γ}, of these 10 amino acids. In contrast, amino acids synthesized by the linear enzymatic reactions have fewer glucose C1-derived carbons. From pyruvate C3, the side chain ends of Ala, Val, and Leu are labeled. Gly loses the glucose C1 label in its synthesis from 3-phosphoglycerate, which also generates Ser and Cys with

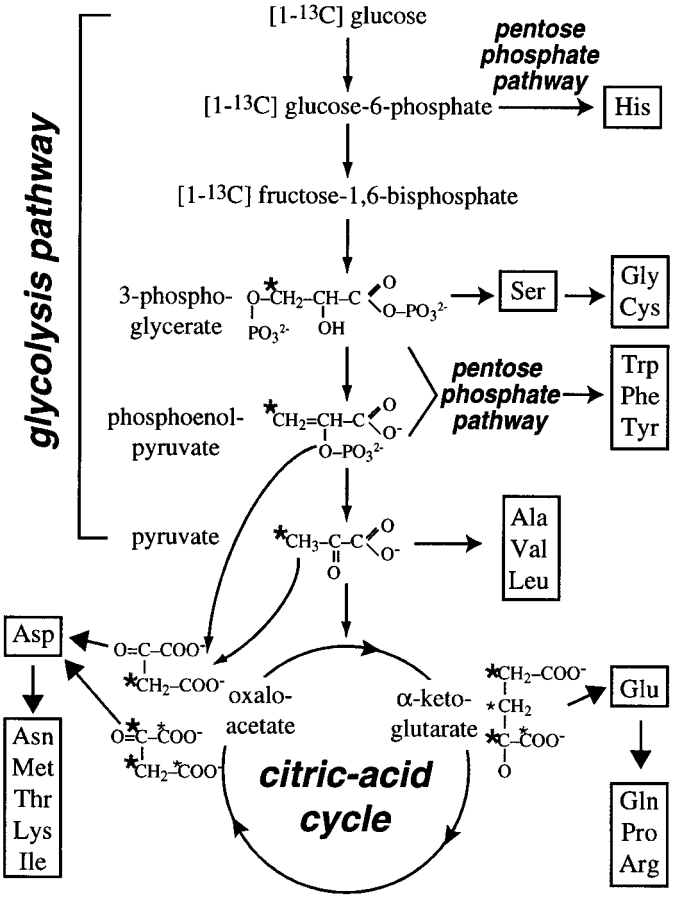

FIG. 1. Amino acid biosynthetic pathways in bacteria, illustrating selective and extensive ^{13}C labeling of proteins. Most compounds in the pathways are precursors for the 20 amino acids. The fate of the glucose C1 is traced. The resulting labeled carbons in the amino acid precursors are designated by asterisks. The smaller asterisks in oxaloacetate and α-ketoglutarate indicate lower labeling levels.

labeled side chain ends. The 3 aromatic amino acids are produced from phosphoenolpyruvate via the pentose phosphate pathway and are labeled at C^{β} and several ring positions.

Therefore, we can obtain a protein that is selectively labeled in ^{13}C by supplementing the bacterial growth media with ^{13}C specifically labeled glucose such as [1-^{13}C]glucose. The absence of labeling for certain sites will alleviate the line broadening, spin diffusion, and dipolar truncation problems mentioned above. The chemical symmetry of the glucose molecule can be exploited to control the maximum labeling level to 50%. Thus, the probability of a ^{13}C spin pair is at most 25% even for two directly bonded labeled sites. This further reduces the influence of the undesirable *J*-couplings. For amino acids produced from the citric-acid cycle, the labeling levels of many sites are reduced to ~25% due to the loss of some ^{13}C labels as CO_2 and the distribution of labels between chemically indistinguishable sites by two symmetric intermediates (succinate and fumarate) of the cycle. The lower labeling levels compensate for the extensiveness of labeling in these amino acids. When a labeling

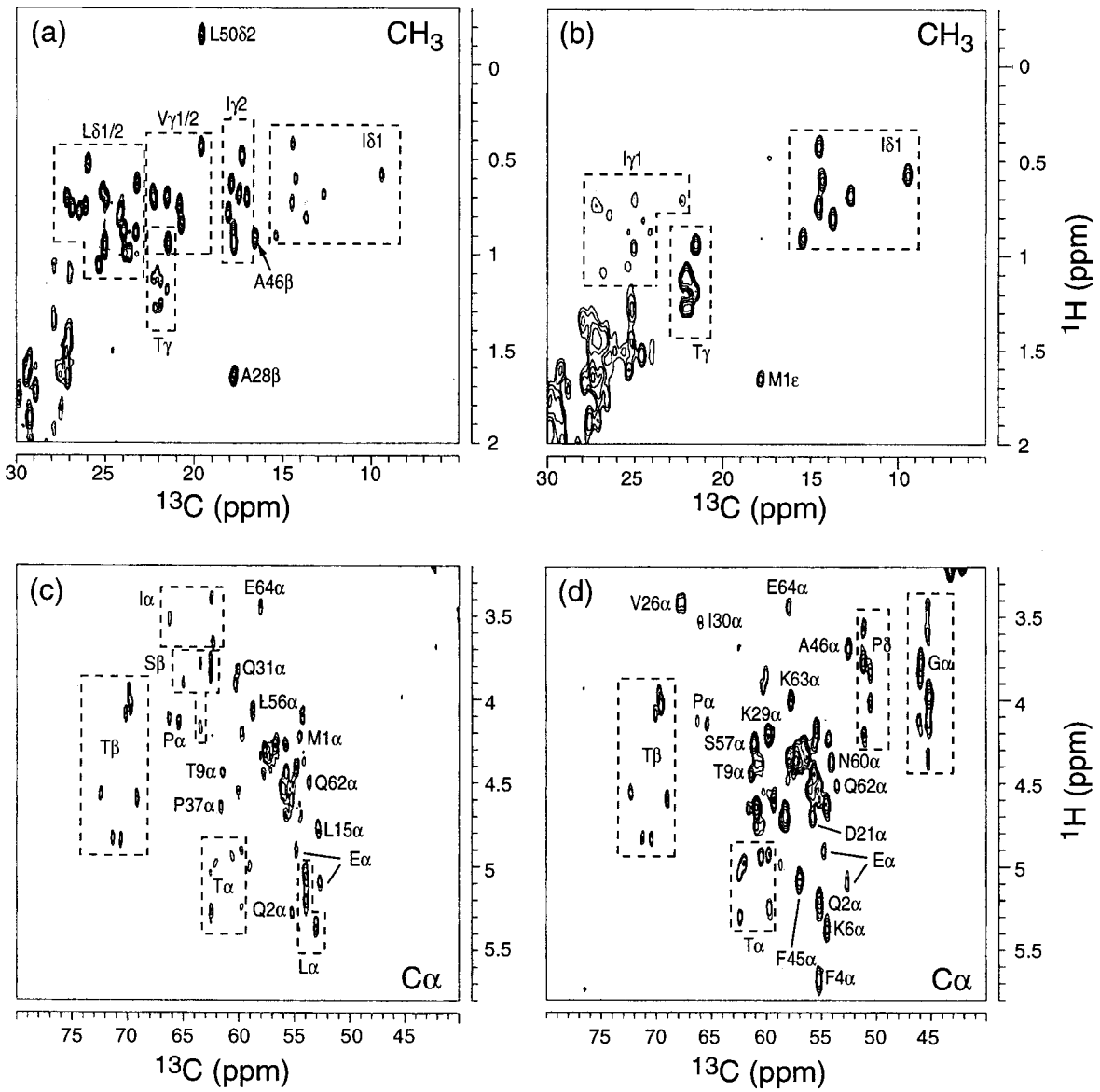

FIG. 2. Solution NMR ^{13}C–^{1}H heteronuclear correlation spectra of $^{13}C1$-ubiquitin and $^{13}C2$-ubiquitin, verifying the selective and extensive ^{13}C labeling patterns. (a) CH_3 region of $^{13}C1$-ubiquitin. (b) CH_3 region of $^{13}C2$-ubiquitin. (c) C^{α}–H^{α} region of $^{13}C1$-ubiquitin. (d) C^{α}–H^{α} region of $^{13}C2$-ubiquitin. Spectral assignment is based on the known chemical shifts of this protein (*27*) and is indicated for some peaks to illustrate the selectivity of the labeling and the partial complementary nature of the $^{13}C1$ and $^{13}C2$ labeling schemes. Areas of the same type of carbons are enclosed by dashed lines.

level of 100% is desired, [1, 6-^{13}C]glucose may be used. This selective labeling approach can also be extended to specifically labeled glycerol and pyruvate, which undergo similar enzymatic reactions and have been used in several solution NMR studies of protein dynamics (*22, 23*).

To demonstrate this selective and extensive ^{13}C labeling approach, we obtained two ubiquitin samples that were expressed from bacterial media supplemented with [1-^{13}C]glucose and [2-^{13}C]glycerol as the sole carbon source. To verify and compare the distribution of ^{13}C-labeled sites, we employed 2D ^{13}C–^{1}H correlation experiments on these samples dissolved in aqueous solution (Fig. 2). The labeled carbon sites were identified by using the solution NMR chemical shifts known for this protein (*27*) and are compiled in Tables 1 and 2. As expected, the two labeling schemes exhibit partial complementarity, in that many sites labeled by [1-^{13}C]glucose are not labeled by [2-^{13}C]glycerol, and vice versa. For example, in the [1-^{13}C]glucose-derived ubiquitin (heretofore referred to as $^{13}C1$-ubiquitin), most side chain methyl carbons are labeled without directly bonded ^{13}C neighbors (Fig. 2a). In comparison, the [2-^{13}C]glycerol-derived ubiquitin (heretofore referred to as $^{13}C2$-ubiquitin) exhibits poor methyl carbon labeling except for Ile $C^{\delta}1$ and Thr C^{α} (Fig. 2b). The isolated methyl carbon labels are potentially useful for measuring long-range ^{13}C–^{15}N and ^{13}C–^{13}C distances between residues to constrain the protein tertiary structure. The [2-^{13}C]glycerol scheme pref-

TABLE 1
^{13}C Labeling Pattern of [1-^{13}C]Glucose

Residue	^{13}C labels		Residue	^{13}C labels	
	Theory	Expt.		Theory	Expt.
Gly	None	None	Glu	[CO[a]], α, β, γ, −	α, β, γ
Cys[b]	β	N.A.	Gln	[CO[a]], α, β, γ, −	α, β, γ
Ser	β	β	Pro	[CO[a]], α, β, γ, −	α, β, γ, −
Ala	β	β	Arg	[CO[a]], α, β, γ, −, −	α, −, γ, −, −
Leu	α, δ1, δ2	α, δ1, δ2	Asp	[CO[a]], α, β, [γ[a]]	α, β
Val	γ1, γ2	γ1, γ2	Asn	[CO[a]], α, β, [γ[a]]	α, β
His	CO[1]	δ2	Met	[CO[a]], α, β, [γ]	α, β, −
Phe	β, δ1, δ2	β, γ, δ1, δ2	Thr	[CO[a]], α, β, [γ]	α, β, [γ]
Tyr	β, δ1, δ2	β, δ1, δ2, ζ	Lys	−, β, [γ], δ, ϵ	−, β, δ, ϵ
Trp[b]	β, δ1, δ2	N.A.	Ile	[CO[1]], α, −, γ1 γ2, [δ1]	α, −, γ1, γ2, [δ1]

Note. The theoretically predicted labeled sites are compared with the experimentally observed ones obtained from the solution NMR data in Fig. 2a. For amino acids produced from the citric-acid cycle (right half of the table), two types of labeling levels are predicted: the normal level of ~50% (no brackets), and a lower labeling level of ~25% (square brackets). The experimental peak intensities, classified as strong (no brackets) and weak (square brackets), agree well with the theoretical predictions. For amino acids produced from the citric-acid cycle, dashes are used to indicate the unlabeled sites.

[a] Carbon sites predicted to be labeled but cannot be confirmed by the ^{13}C–^{1}H correlation experiment due to the lack of directly bonded protons.

[b] Amino acids not present in ubiquitin. The experimental data are not available (N. A.).

erentially labels the $^{13}C^{\alpha}$ of the linear-chain amino acids, while the [1-^{13}C]glucose scheme does not. Isolated $^{13}C^{\alpha}$ sites are useful for measuring ϕ torsion angles to directly probe the protein secondary structure. Those amino acids with both $^{13}C^{\alpha}$ and ^{13}CO labels are suitable for ψ torsion angle measurements using the NCCN technique (*28, 29*) and techniques that correlate the ^{13}CO chemical shift anisotropy with the $^{13}C^{\alpha}$–$^{1}H^{\alpha}$ dipolar coupling (*30, 31*).

Overall, the predicted labeling patterns are borne out well by the solution NMR spectra, as shown in Tables 1 and 2. No comparison is made for the two missing amino acid types in ubiquitin and for the unprotonated carbons, which are not detectable by the experiment. The good agreement between the experiment and the prediction indicates that label scrambling is negligible. Based on residual signals of glycine C^{α} in the ^{15}N–^{13}C correlation spectra of ^{13}C1-ubiquitin (Fig. 6), we estimate that scrambling contributes ~10% of the labeling. Low scrambling is crucial for securing the selectivity of labeling, especially for amino acids produced from the linear part of the biosynthetic pathways. If desired, the more extensive labeling

TABLE 2
^{13}C Labeling Pattern of [2-^{13}C]Glycerol

Residue	^{13}C labels		Residue	^{13}C labels	
	Theory	Expt.		Theory	Expt.
Gly	α	α	Glu	[CO[a]], (α), [β], −, δ[a]	[α], [β], −,
Cys[b]	α	N. A.	Gln	[CO[a]], (α), [β], −, δ[a]	[α], [β], −
Ser	α	α	Pro	[CO[a]], (α), [β], −, δ	[α], [β], −, δ
Ala	α	α	Arg	[CO[a]], (α), [β], −, δ	[α], [β], −, δ
Leu	CO[a], β, γ	β, γ	Asp	[CO[a]], [α], (β), [γ[a]]	[α], [β]
Val	α, β	α, β	Asn	[CO[a]], [α], (β), [γ[a]	[α], [β]
His	α	δ2	Met	[CO[a]], [α], (β), [γ]	[α], −, [γ], ϵ
Phe	α, γ, ϵ1	α, γ, ϵ1	Thr	[CO[a]], [α], (β), [γ]	[α], [β], γ
Tyr	α, γ, ϵ1	α, γ, ϵ1, ζ	Lys	α, −, [γ], (δ), [ϵ]	α, −, γ, [δ], ϵ
Trp[b]	α, δ2, ζ3	N. A.	Ile	[CO[a]], [α], β, (γ1), [δ1]	[α], [β], [γ1], δ1

Note. The theoretically predicted labeled sites are compared with the experimentally observed ones obtained from the solution NMR data in Fig. 2b. For amino acids produced from the citric-acid cycle, three types of labeling levels are predicted: the normal labeling level is ~100% sites in square brackets are labeled at ~50%, and sites in round brackets are labeled at <25%. The experimental peak intensities, classified as strong (no brackets) and weak (square brackets), show general agreement with the theoretical predictions. For amino acids produced from the citric-acid cycle, dashes are used to indicate the unlabeled sites.

[a] Carbon sites predicted to be labeled but cannot be confirmed by the ^{13}C–^{1}H correlation experiment due to the lack of directly bonded protons.

[b] Amino acids not present in ubiquitin. The experimental data are not available (N. A.).

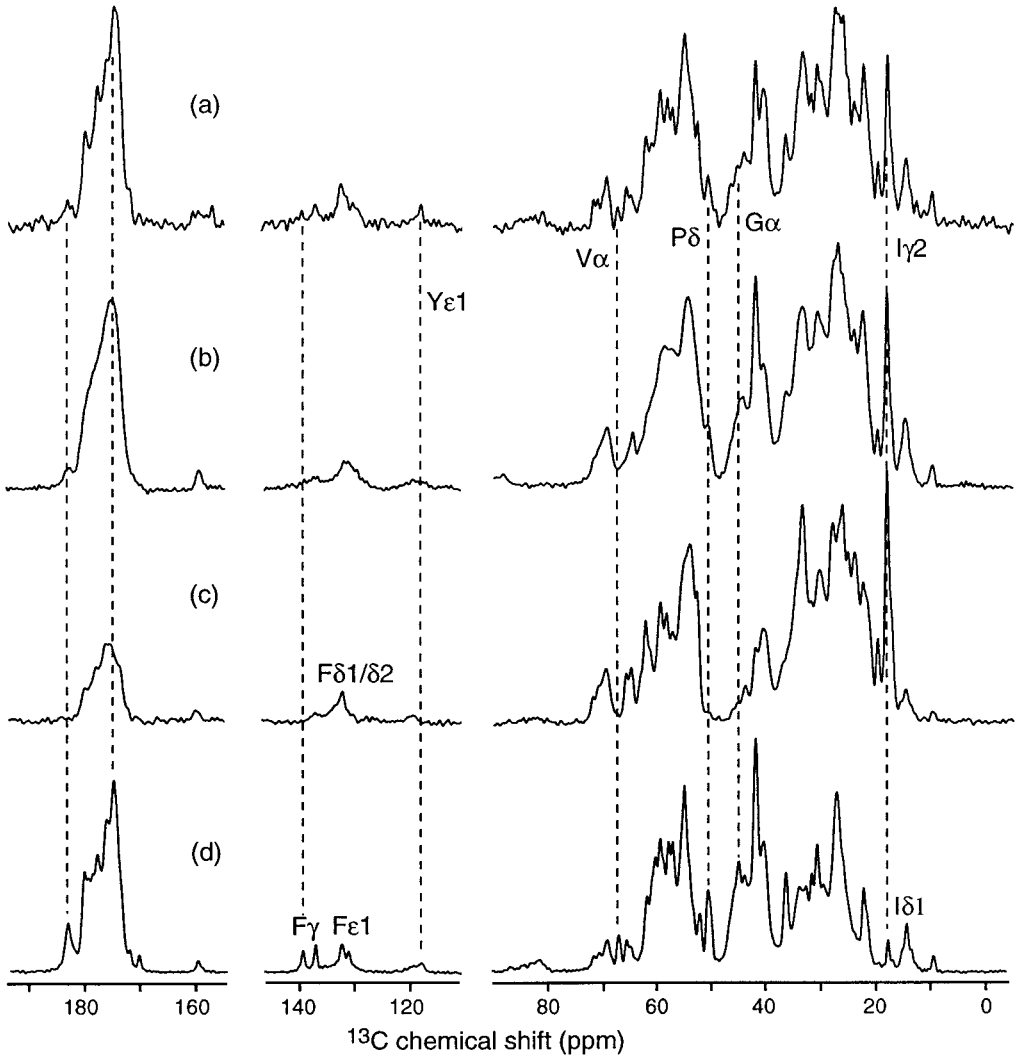

FIG. 3. Solid-state ^{13}C CPMAS spectra of differently labeled ubiquitin samples. (a) Unlabeled ubiquitin, 35 mg, 4096 scans. (b) [U-$^{13}C_6$]glucose, ^{15}N-labeled ubiquitin, 10 mg, 64 scans. (c) [1-^{13}C]glucose, ^{15}N-labeled ubiquitin, 15 mg, 128 scans. (d) [2-^{13}C]glycerol, ^{15}N-labeled, 20 mg, 128 scans. The different intensity distributions of spectra (c) and (d) compared to (a) and (b) reflect the selectivity of labeling. Assignments for several resolved signals are indicated to illustrate the effects of selective labeling. Spectrum (b), of the uniformly labeled sample, has the lowest resolution due to the ^{13}C–^{13}C scalar couplings and the residual dipolar interaction.

of the amino acids from the citric-acid cycle can be avoided by supplementing the minimal medium with unlabeled intermediates of the citric-acid cycle or the unlabeled amino acid products themselves (*32*).

The selective and extensive ^{13}C labeling approach (*22*, *23*) differs from other selective labeling methods that require bacterial auxotrophs (*33*–*35*) and from random fractional labeling (*36*, *37*). It is easy to implement with the standard protein expression protocol and is very versatile, since specifically ^{13}C-labeled glucose, glycerol, and pyruvate are commercially available in many forms. The feasibility and versatility of this labeling approach, together with the resulting potential efficiency in the NMR structure determination, compensate for the reduced control in the placement of the isotopic labels compared to site-specific labeling methods.

2. One-Dimensional ^{13}C NMR Spectra of Selectively Labeled Ubiquitin

To demonstrate the effects of S&E ^{13}C labeling on the resolution of the solid-state NMR spectra and to estimate the labeling levels, we acquired 1D ^{13}C CPMAS spectra of four different ubiquitin samples. The spectrum of the unlabeled ubiquitin (Fig. 3a) serves as a reference to those of the labeled samples in three ways. First, its intensity distribution is a fingerprint of the complete carbon skeleton of the protein, since all carbons in the molecule contribute equally at the natural abundance (1.1%) level. Deviations from this total intensity distribution would thus reflect the preferential labeling of certain carbon sites. Second, the homogeneous linewidth of the spectrum is minimal at the natural abundance, since the effects

of the ^{13}C–^{13}C scalar couplings and residual dipolar couplings are absent. Third, the signal-to-noise ratio of the spectrum provides a benchmark against which the labeling levels of the [1-^{13}C]glucose and [2-^{13}C]glycerol schemes can be estimated.

For U-^{13}C, ^{15}N-labeled ubiquitin, the spectrum (Fig. 3b) exhibits significant line broadening, as expected when residual ^{13}C–^{13}C dipolar and scalar couplings are present. This dipolar- and scalar-coupling induced line broadening was also reported recently for crystalline organic compounds (*14, 38*). It was found that to remove the effects of these couplings, very high spinning speeds (>25 kHz) and proton decoupling fields (~200 kHz) needed to be employed. These experimental conditions are currently only feasible on the smallest MAS rotors, which have limited sample volumes and thus reduced experimental sensitivity. In addition, such high spinning speeds make rotor-synchronized NMR pulse sequences difficult to implement.

Under [1-^{13}C]glucose labeling, the ubiquitin spectrum (Fig. 3c) exhibits reduced intensities than the reference spectrum in the Cα region between 50 and 65 ppm and at ~40 ppm. In comparison, the [2-^{13}C]glycerol labeling scheme yields low intensities in the side chain region between 15 and 35 ppm (Fig. 3d). These different intensity distributions reflect the selectivity of labeling. For example, the Gly and Val $^{13}C^{\alpha}$ peaks are conspicuously missing in the $^{13}C1$-ubiquitin spectrum, while the Ile $^{13}C^{\gamma}2$ carbons are mostly unlabeled in $^{13}C2$-ubiquitin. (These resonances are assigned based on the solution NMR data (*27*) and are confirmed by the 2D ^{15}N–^{13}C spectra shown later.) In the carbonyl region, $^{13}C2$-ubiquitin displays substantially higher intensities, suggesting that the carbonyl carbons are labeled at higher levels than in $^{13}C1$-ubiquitin. In general, based on the relative intensities of the $^{13}C1$- and $^{13}C2$-ubiquitin spectra to the reference spectrum (Fig. 3a), and taking into account the sample amounts and signal-averaging times, we find approximately a factor of 2 enhancement in the labeling levels of the [2-^{13}C]glycerol scheme (50–90%) over the [1-^{13}C]glucose scheme (20–45%). This is consistent with the predictions based on the amino acid biosynthetic pathways.

Both selectively labeled ubiquitin samples exhibit sharper resonances than the uniformly labeled sample. The linewidths in spectra (c) and (d) range from 0.8 ppm for the unprotonated carbonyl carbons and the mobile methyl carbons, to ~1.3 ppm for the CH and CH_2 groups. In contrast, the fully labeled sample under the same experimental conditions exhibits linewidths of ~1 ppm for CH_3 groups and >2 ppm for CH_2 carbons. These linewidth differences confirm the importance of reducing directly bonded ^{13}C spin pairs for obtaining highly resolved solid-state NMR spectra.

3. Site-Specific Determination of Multiple ϕ Torsion Angles by HNCH Correlation

The high spectral sensitivity and resolution achieved with S&E ^{13}C labeling makes possible a variety of solid-state 2D correlation techniques for measuring structural constraints such as torsion angles (*24, 28, 30, 31, 39, 40*) and for sequential resonance assignment (*41–43*). We first demonstrate the feasibility of residue-specific torsion-angle determination on such a selectively labeled protein by measuring backbone ϕ angles in $^{13}C2$-ubiquitin. The recently introduced HNCH technique correlates the N–H and the C^{α}–H^{α} dipolar coupling tensors (*24*) in order to extract the mutual orientation of the two bonds, which reflects the ϕ torsion angle about the N–C^{α} bond. The ϕ-dependent dipolar patterns are manifested in the ω_1 dimension and separated in the ω_2 dimension according to the C^{α} isotropic chemical shifts of the residues. Due to this isotropic–anisotropic correlation, the HNCH technique is capable of extracting multiple ϕ torsion angles simultaneously, provided that the $^{13}C^{\alpha}$ chemical shift dispersion is sufficient.

The HNCH spectrum of $^{13}C2$-ubiquitin is displayed in Fig. 4. The projection onto the ω_2 dimension and the ω_1 cross sections of four selected sites are shown. In the ω_2 dimension, only carbons directly bonded to nitrogen spins, i.e., C^{α} and CO, are observed, since a short ^{15}N–^{13}C double- and zero-quantum excitation time was used (0.47 ms). In the ω_1 dimension, only the intensity envelopes connecting the tips of the sidebands are plotted in order to emphasize the ϕ-angle-induced differences in the intensity distribution. The spectra consist of 14 sidebands and one center band, as determined by the number of t_1 intervals measured. The dipolar cross section of Val26 C^{α} (67 ppm) displays a dip in the central intensity and is best-fit with $\phi = -60°$ (Fig. 4b). This corresponds to the α-helix conformation, which is in agreement with the crystal structure (*17*). The dipolar cross section of Thr12 and Thr14 C^{α} (62 ppm) is dominated by a sharp intensity maximum at the center, which is the signature for the β-sheet conformation (Fig. 4c). The Ala46 (53 ppm) cross section exhibits a broad high plateau in the center and corresponds to $\phi = +20°$ or $+100°$, both suggesting a β-turn structure (Fig. 4d). This is also corroborated by the crystal structure (*17*). Even in the absence of the crystal structure, this result, combined with the fact that Gly47 is the neighboring residue, would strongly suggest a type I′–III′ β-turn (*44*).

The experimental spectra are each best fit (Figs. 4b–4d, right) with two ϕ-torsion angles because the HNCH technique has an intrinsic double degeneracy (*24*). However, one of these two angular values can often be ruled out based on its rare occurrence in nature (*45*). The best-fit simulations are found at the minimal root-mean-square deviations (rmsd) between the normalized experimental spectrum $S_{i,\mathrm{exp}}$ and the normalized simulated ones $S_i(\phi)$. The rmsd curve is calculated according to

$$\mathrm{rmsd}(\phi) = \left\{ \frac{1}{N} \sum_{i=1}^{N} [S_{i,\mathrm{exp}} - S_i(\phi)]^2 \right\}^{1/2}, \qquad [1]$$

where the summation i is carried out over the central six

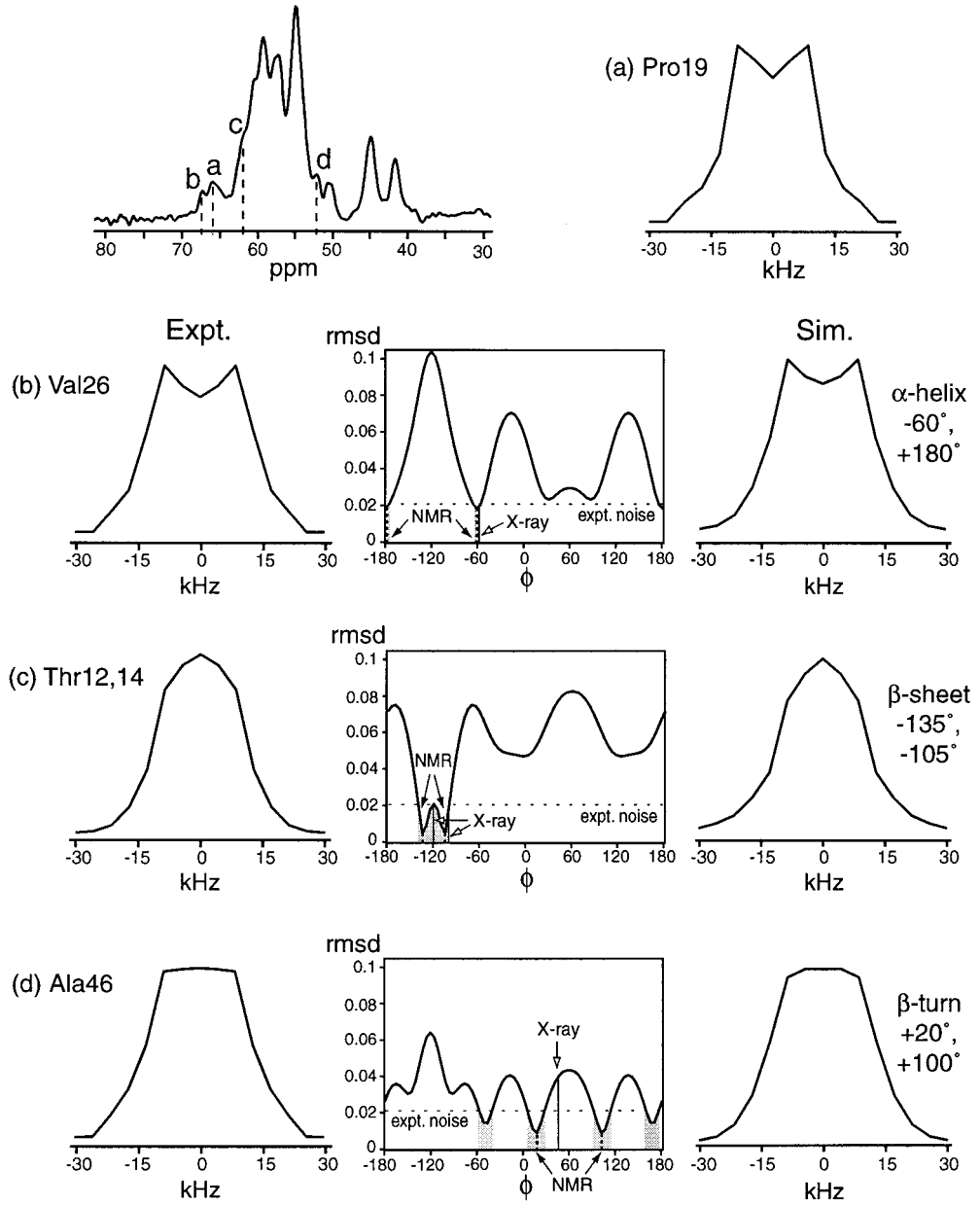

FIG. 4. HNCH spectrum of ^{13}C2-ubiquitin for determining the ϕ torsion angles. The experimental dipolar cross sections (ω_1 dimension) are the C$^{\alpha}$ of (a) Pro19, (b) Val26, (c) Thr12 and Thr14, and (d) Ala46. The assignment is obtained from solution NMR data (*27*) and is confirmed by the solid-state ^{15}N–^{13}C 2D correlation spectra. The root-mean-squared deviations (rmsd) between the experiment and simulation are displayed in the middle column of (b–d). The best-fit torsion angles (dashed lines) are obtained at the minimum rmsd value. The experimental uncertainties are indicated by the shaded areas. The crystal structure results are indicated by the solid lines. For cross section (c), two solid lines are shown that correspond to Thr12 ($\phi = -120°$) and Thr14 ($\phi = -101°$). The best-fit simulations are shown in the right column of (b–d). The effective C–H dipolar coupling can be extracted from the Pro19 slice (a) due to its lack of the amide proton. The sample was spun at 4209 Hz. A ^{15}N–^{13}C coherence transfer time of 475 μs was used to select carbons directly bonded to the amide ^{15}N. The spectrum was acquired in 14 h.

spinning sidebands and the center band in each spectrum (*46*). The outer eight side bands were excluded in the rmsd calculation since their intensities are low and relatively similar for various ϕ angles. The global minima of each rmsd curve correspond to the best-fit torsion angles. A pair of minima is present for each rmsd curve, which reflects the double degeneracy of the HNCH technique. For the α-helix (b) and β-turn (d) conformations, an additional pair of angles exhibit near-minimum rmsd values. This results from an accidental, near fourfold degeneracy in these angular regions, which has been observed in 2D (ϕ, ϕ) rmsd plots previously (*46*).

To assess the angular resolution of the technique, we measured the experimental noise and used its intersection with the rmsd curve to define an angular uncertainty (shaded areas).

Based on this criterion, the Val26 spectrum has the highest angular resolution, while the Ala46 result is the least precise. The accuracy of the NMR measurement can also be assessed, by comparing the NMR-derived torsion angle values (dashed lines) with the crystal structure (solid lines). We find relatively high accuracy for the α-helical and β-sheet conformations, but low accuracy for the positively valued, β-turn conformation. This may partly result from the fact that the C^{α} signal of Ala46 is not sufficiently resolved from other sites. It is also possible that the flexibility of the β-loop makes the NMR or the X-ray crystal structure an average of a number of conformations.

An internal check for the precision of the HNCH experiment is provided by the dipolar cross sections of the chemically unique amino acid, proline. Due to the lack of the amide proton in proline, its HNCH cross section exhibits a narrow envelope (Fig. 4a) that reflects the effective C^{α}–H^{α} dipolar coupling scaled by the homonuclear decoupling sequence. Knowledge of this effective C–H coupling makes the HNCH simulation independent of any adjustable parameter other than the torsion angle ϕ.

The advantage of the selective and extensive ^{13}C labeling scheme compared to uniform ^{13}C labeling lies in the fact that the uniformly labeled sample has practically no single-site resolution in the C^{α} region to yield any useful HNCH spectrum. Although higher spinning speeds could improve the chemical shift resolution, they are incompatible with the HNCH sequence, which requires a sufficient number of t_1 points as defined by the MREV-8 cycle time to be measured within each rotor period. This slow-spinning requirement is the main limitation of the torsion-angle technique, because even with the enhanced resolution afforded by ^{13}C selective labeling, the ω_2 dimension still does not resolve all C^{α} resonances. To extract more torsion angles, it is necessary to extend the 2D HNCH technique into a third dimension, where ^{15}N chemical shift may be employed to further disperse the resonances. This 3D experiment should not entail prohibitively long signal-averaging time, since the dipolar dimension of the experiment, incremented in a constant-time fashion (*24*), requires only a small number of points to be measured.

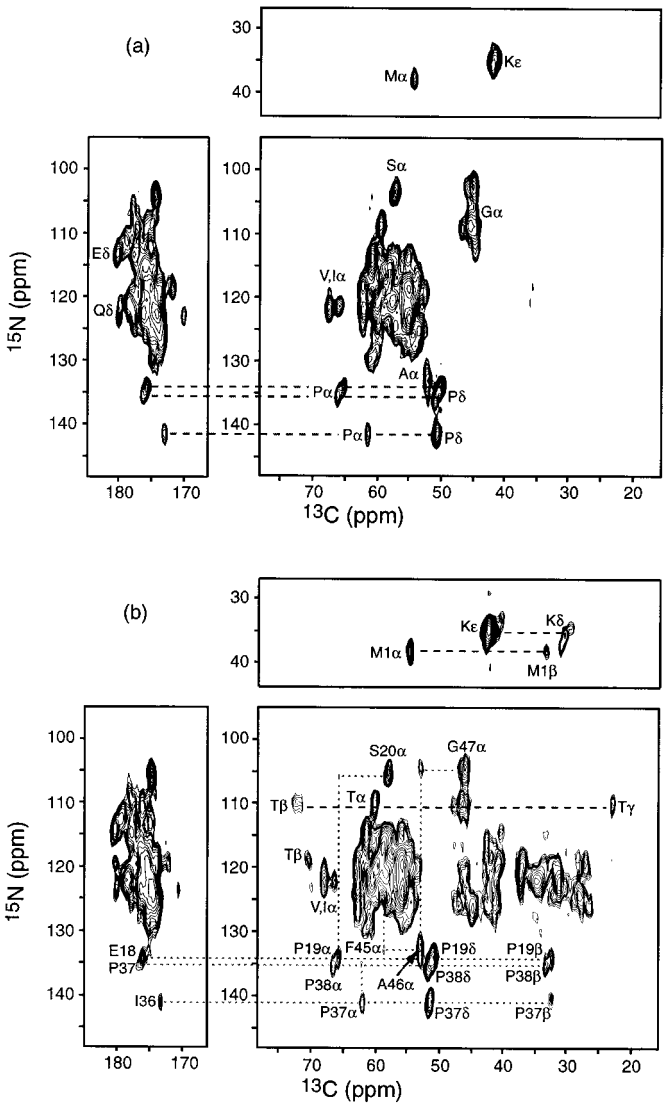

FIG. 5. ^{15}N–^{13}C 2D correlation spectrum of $^{13}C2$-ubiquitin with a ^{15}N–^{13}C mixing time of (a) 0.6 ms and (b) 2.3 ms. Several dozens of resonances are either partially or completely resolved in each spectrum. Amino-acid type assignment and partial sequential assignment were achieved based on the connectivity patterns, the characteristic chemical shifts, and the labeling patterns derived from Fig. 2 and Tables 1 and 2. The spectra were each acquired in 13 h.

4. Resonance Assignment by ^{15}N–^{13}C Correlation

The structure elucidation of extensively labeled proteins by NMR requires the assignment of the measured structural constraints to the protein sequence (*47*). So far, solid-state NMR techniques for resonance assignment have been demonstrated mainly on small molecules such as amino acids and oligopeptides (*42, 48–51*), and few solid-state NMR studies of resonance assignment for proteins have been shown (*41, 43, 52*). The S&E ^{13}C labeling approach facilitates resonance assignment by enhancing the spectral resolution. As a first demonstration of this feasibility, we carried out a 2D ^{15}N–^{13}C correlation experiment (*42*) where the coherence is transferred between ^{13}C and ^{15}N via the recoupled dipolar interaction (*53*). The spectra yield sequence-specific assignment based on $-N_i-C^{\alpha}{}_i-N_{i+1}-C^{\alpha}_{i+1}-$ and $-N_i-CO_i-N_{i+1}-CO_{i+1}-$ connectivities. Due to the distance-dependent nature of this coherence transfer mechanism, one can first identify the N–C^{α} and CO_{i-1}–N_i cross peaks by using a short ^{15}N–^{13}C mixing time, then identify two- and three-bond ^{15}N–^{13}C spin pairs such as the intraresidue N–C^{β} and the interresidue C^{α}_{i-1}–N_i peaks using a longer mixing time (*42*).

We applied this ^{15}N–^{13}C correlation technique to $^{13}C2$-ubiquitin. Two ^{15}N–^{13}C spectra, acquired with a ^{15}N–^{13}C mixing time of 0.6 and 2.3 ms, are displayed (Fig. 5). Each spectrum yields several dozens of resonances that are either partially or completely resolved. Based on the chemical shifts, the connec-

tivity patterns, the labeling pattern specific to this sample, and the time-dependence of the resonance signals, we can identify several sequential connectivities. For example, in the spectrum acquired with the short mixing time (a), the six most downfield ^{15}N resonances can be assigned to prolines due to their characteristic chemical shifts. Among these peaks, the signals at ^{13}C chemical shifts of ~50 ppm can be assigned to proline C^{δ}, while those at ~62 and ~67 ppm are proline C^{α}. Both C^{δ} and C^{α} are labeled by the [2-^{13}C]glycerol scheme and are directly bonded to the amide ^{15}N, thus they are observed at the short mixing time. At this point, only type assignment is possible. When the longer ^{15}N–^{13}C mixing time is used, we observe a weak but clear cross peak between two of the three proline C^{α} resonances. This unambiguously assigns the two peaks to the two consecutive prolines in the ubiquitin sequence, Pro37 and Pro38. Thus the remaining proline signals must belong to Pro19. One can continue along the connectivity pattern to identify the cross peak between Pro37 and Ile36, as well as the Pro19–Ser20 cross peak. Another observed sequential connectivity is Gly47–Ala46–Phe45 (*43*). In addition to interresidue assignment, the long mixing-time experiment also allows intraresidue assignment to be made to some extent, since the sidechain resonances appear in the same ^{15}N cross section as the primary C^{α} signal but have more upfield ^{13}C chemical shifts. One example of the intraresidue assignment is provided by the prolines, whose C^{β} site, two bonds from the amide ^{15}N, is clearly shown in Fig. 5b. Similarly, the Thr C^{β}'s and C^{γ}'s can also be assigned, since Thr C^{β}'s have uniquely downfield chemical shifts. These assignments were made based on the solid-state spectra alone, without utilizing solution NMR chemical shift information. The latter, however, is useful as an eventual measure of the uniqueness of the solid-state assignment given the achievable linewidths (*41*). In these spectra, the limiting values of the full width at half maximum are ~0.8 ppm for ^{13}C and ~2.5 ppm for ^{15}N. This resolution is quite reasonable for an unoriented powder sample and is reflected by the partial separation of the six glycine resonances in the spectra.

Although the selective ^{13}C labeling makes complete assignment from a single sample not possible, with two samples labeled in a complementary fashion, one can retrieve the missing information to some extent. For example, the ^{13}C1-ubiquitin spectrum acquired at the long ^{15}N–^{13}C mixing time (Fig. 6b) exhibits the C^{β} signals of Ala, Ser, and Pro. Among these, Ser20 C^{β} can be assigned based on its cross peak with Pro19 C^{α}, and Ala46 C^{β} is identified by its cross peak with Gly47 C^{α}. Thr9 can be assigned by its cross peak with Leu8 C^{α}. Similarly, the sequential connectivities Thr66–Ser65 and Pro19–Glu18 can be identified.

To assign the ^{13}C and ^{15}N spectra of a solid protein more completely, additional correlation experiments that fully exploit the labeling patterns are required. For example, 3D experiments that correlate the C^{α} and sidechain carbon chemical shifts with the backbone ^{15}N are useful for more complete amino acid type assignment of the resonances. Homonuclear ^{13}C correlation schemes will also be useful for type assignment. Experiments along these lines will be detailed in a future paper (*54*). On the other hand, variations of the selective and extensive labeling approach can be exploited to label carbons that are either unlabeled or labeled at low levels by the [1-^{13}C]glucose and [2–^{13}C]glycerol labeling schemes. This will be important to achieve complete resonance assignment of the proteins.

CONCLUSIONS

We have shown that selective and extensive ^{13}C labeling in conjunction with high-resolution solid-state NMR is a useful approach to the efficient structure investigation of solid proteins. The selective ^{13}C labeling primarily refers to the fact that the statistical probability of directly bonded ^{13}C–^{13}C spin pairs is close to 0% while the probability of one of the two carbons being ^{13}C is significant. This is achieved by using specifically labeled glucose or glycerol as the sole carbon source in the bacterial growth media. We found, both theoretically and experimentally, that the selectivity of labeling is most prominent for the 10 amino acids produced from the linear part of the biosynthetic pathways. In these amino acids, many carbon pairs with 45–90% and 1.1% (i.e., natural abundance) labeling levels are found. In comparison, in amino acids derived from the more complex citric-acid cycle, many adjacent carbons have 50% or lower labeling levels for both sites, thus the spin-pair probabilities are below 25%.

The selective and extensive ^{13}C labeling approach provides a general method of spectral narrowing and editing, which facilitates resonance assignment in solid proteins. The enhanced spectral resolution makes many solid-state NMR techniques practical for measuring multiple structural constraints per experiment and per sample. We showed here that constraints on the backbone conformation of such a labeled protein can be obtained by measuring the ϕ torsion angles using the HNCH technique. The angular resolution and accuracy of the measurement were analyzed. We also showed that the sequence-specific assignment of these structural constraints is partially feasible by 2D ^{15}N–^{13}C correlation. The extent of resonance assignment is still limited at this point by the spectral resolution due to the lack of ultrafast spinning and ultrahigh magnetic field. Combining the advance of these technologies, various heteronuclear and homonuclear correlation techniques, and 3D spectroscopy, more complete resonance assignment of proteins in the solid state is well foreseeable.

MATERIALS AND METHODS

The three ^{13}C, ^{15}N-labeled ubiquitin samples used in this work were custom-synthesized by VLI-Research (Malvern, PA). The human ubiquitin gene was expressed in *Escherichia coli.* Cells were grown in M9 minimal medium, with the sole nitrogen source being ^{15}N-labeled ammonium sulfate, and the sole carbon source being one of the following three com-

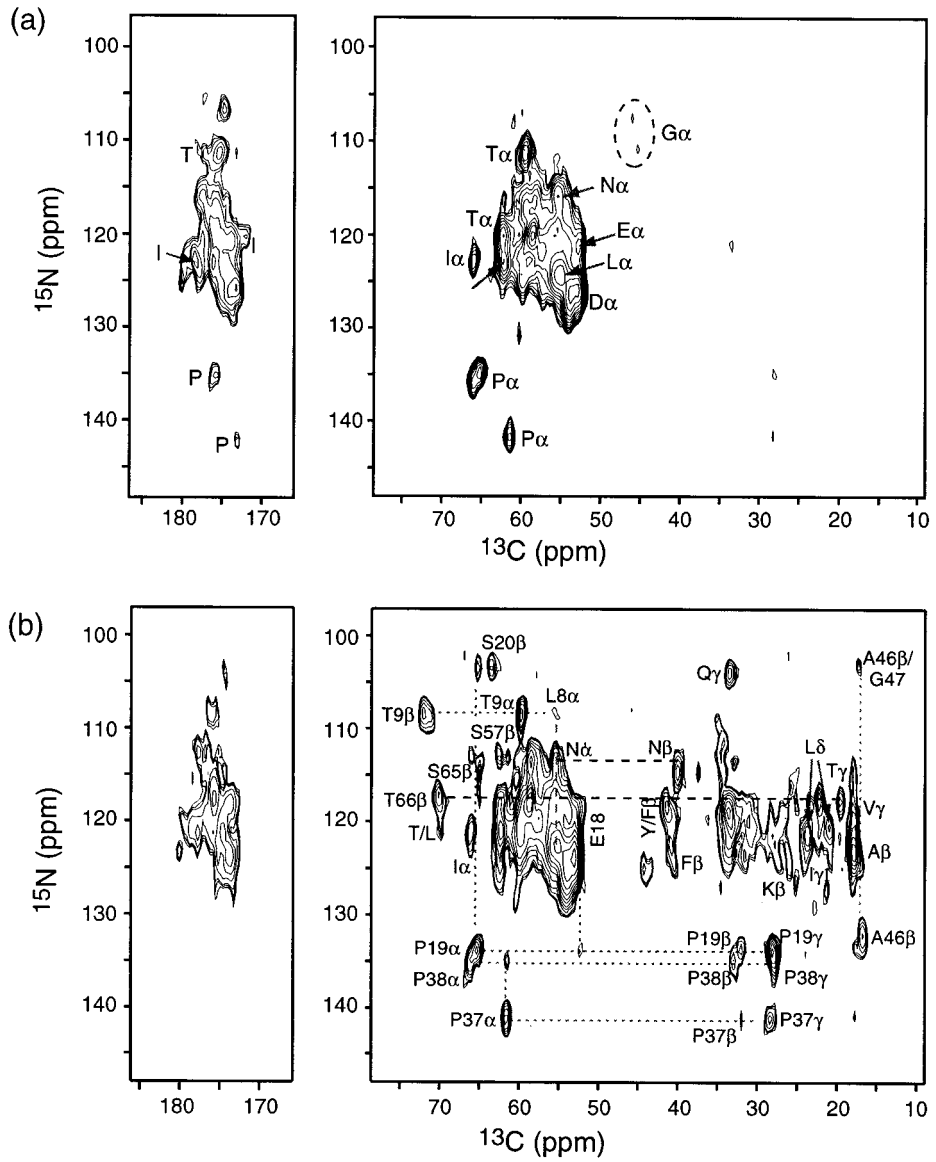

FIG. 6. ^{15}N–^{13}C 2D correlation spectrum of ^{13}C1-ubiquitin with a ^{15}N–^{13}C mixing time of (a) 0.6 ms and (b) 2.3 ms. Dashed circle indicates the weak glycine C^{α} signals, whose presence indicates low-level scrambling in the ^{13}C labeling scheme.

pounds: [1-^{13}C]glucose, [2-^{13}C]glycerol, and [U-$^{13}C_6$]glucose (Cambridge Isotope Labs, Inc.). For a typical ubiquitin expression experiment, a 5-liter culture was induced and the solid paste was purified by column chromatography to homogeneity. The purity of the final products was analyzed by gel electrophoresis and amino acid composition analysis to be >99%. The unlabeled ubiquitin sample was purchased from Sigma and used directly without purification. All samples were hydrated to ~30% (w/w) prior to the NMR experiments. Hydration was found to be important for narrowing the spectral lines, mainly by decreasing the conformational heterogeneity present in lyophilized samples (*55–57*).

The solution-state ^{13}C–^{1}H 2D correlation experiments for verifying the labeling schemes were carried out on a Bruker DPX-300 spectrometer using a 5-mm inverse probe. A refocused INEPT pulse sequence was used (*58*). The samples consist of 0.7 mM ubiquitin dissolved in a 90% H_2O/10% D_2O sodium acetate buffer at pH 4.5.

All solid-state NMR experiments were performed on a Bruker DSX-300 spectrometer using a 4-mm triple-resonance MAS probe. Typical radiofrequency field strengths were 120 kHz for ^{1}H decoupling, 65 kHz for ^{13}C, and 50 kHz for ^{15}N. Cross polarization from ^{1}H to ^{13}C was achieved with a linearly ramped (*59, 60*) RF field on the ^{13}C channel and with a contact time of 0.5 ms. The FIDs were detected under ^{1}H TPPM decoupling (*61*). The evolution period of the ϕ torsion experiment employed a MREV-8 pulse train for homonuclear decoupling. Otherwise, continuous-wave decoupling was applied on the ^{1}H channel. Typical recycle delays were 3 s.

The 1D ^{13}C CPMAS experiments and the 2D ^{15}N–^{13}C cor-

relation experiments were performed under 7 kHz of magic-angle spinning. The spinning speed was controlled to ±2 Hz by a Bruker MAS controller. The ^{15}N–^{13}C correlation experiments were carried out using the pulse sequence in reference (*42*), except that the ^{15}N–^{13}C REDOR mixing period consisted of a single ^{13}C 180° pulse and multiple ^{15}N 180° pulses (*62, 63*). A total of 4 and 16 rotor periods were used to excite the double- and zero-quantum ^{15}N–^{13}C coherence of one-bond and multiple-bond ^{15}N–^{13}C pairs, respectively.

The ϕ torsion angle experiment was performed using the basic pulse sequence in Ref. (*24*), except that the apparent N–H and C^{α}–H^{α} dipolar couplings were doubled relative to the spinning speed to achieve high angular resolution. The doubling was achieved by moving the 180° pulses on the ^{13}C and ^{15}N channels as a function of t_1 during the constant-time evolution period (*46*). Meanwhile, MREV-8 homonuclear decoupling (*64*) was applied for the entire rotor period on the ^{1}H channel. The MREV-8 90° pulse length was 2.2 μs and the short-window delay was 0.9 μs. They were optimized by maximizing the sideband intensities of the leucine $^{13}C^{\alpha}$ signal detected under MREV-8 decoupling. At a spinning speed of 4209 Hz, 16 t_1 points were collected at an increment of 14.85 μs, so that the maximum evolution time corresponded to one rotor period. Before the t_2 period, a TOSS sequence (*65*) was applied to remove the carbonyl sidebands in the ω_2 dimension, since they overlap with some of the aliphatic resonances.

To eliminate uncertainties in the MREV-8 scaling factor, the magnitude of the one-bond C–H dipolar coupling was directly measured using a DIPSHIFT pulse sequence (*66–68*). The result was further corroborated by the proline C^{α} cross section in the ϕ-angle spectra. The one-bond C–H couplings were thus found to be 10 ± 1 kHz.

The ϕ-angle spectra were simulated using a FORTRAN program described previously (*24*). A long-range C^{α}–H(N) dipolar coupling of 1.2 kHz was taken into account in the simulation. The theoretical ϕ-angle spectra were calculated at 5° increments over the entire 360° range. The root-mean-square deviations between the experiment and the simulations were calculated in MATLAB as a function of the ϕ-angle.

ACKNOWLEDGMENTS

This work was supported by the NSF Materials Research Science and Engineering Center at UMass and by a NSF POWRE grant (MCB-9870373). The author thanks Tauseef Butt for competent expression of the ubiquitin samples and W. Hu for making the MAS simulation program available.

REFERENCES

1. F. Creuzet, A. McDermott, R. Gebhard, K. van der Hoef, M. B. Spijker-Assink, J. Herzfeld, J. Lugtenburg, M. H. Levitt, and R. G. Griffin, Determination of membrane protein structure by rotational resonance NMR: Bacteriorhodopsin, *Science* **251,** 783–786 (1991).
2. K.-J. Shon, Y. Kim, L. A. Colnago, and S. J. Opella, NMR studies of the structure and dynamics of membrane-bound bacteriophage Pf1 coat protein, *Science* **252,** 1303–1305 (1991).
3. R. R. Ketchem, W. Hu, and T. A. Cross, High resolution conformation of Gramicidine A in a lipid bilayer by solid-state NMR, *Science* **261,** 1457–1460 (1993).
4. L. M. McDowell, C. A. Klug, D. D. Beusen, and J. Schaefer, Ligand geometry of the ternary complex of 5-enolpyruvvylshikimate-3-phosphate synthase from rotational-echo double-resonance NMR, *Biochemistry* **35,** 5395–5403 (1996).
5. J. Kummerlen, J. D. vanBeek, F. Vollrath, and B. Meier, Local structure in spider dragline silk investigated by two-dimensional spin-diffusion nuclear magnetic resonance, *Macromolecules* **29,** 2920–2928 (1996).
6. H. W. Long, and R. Tycko, Biopolymer conformational distributions from solid-state NMR: α-helix and 310-helix contents of a helical peptide, *J. Am. Chem. Soc.* **120,** 7039–7048 (1998).
7. J. R. Long, J. L. Dindot, H. Zebroski, S. Kiihne, R. H. Clark, A. A. Campbell, P. S. Stayton, and G. P. Drobny, A peptide that inhibits hydroxyapatite growth is in an extended conformation on the crystal surface, *Proc. Natl. Acad. Sci. USA* **95,** 12083–12087 (1998).
8. K. Schmidt-Rohr and H. W. Spiess, "Multidimensional Solid-State NMR and Polymers," Academic Press, San Diego (1994).
9. G. M. Clore and A. M. Gronenborn, Two-, three-, and four-dimensional NMR methods for obtaining larger and more precise three-dimensional structures of proteins in solution, *Annu. Rev. Biophys. Chem.* **20,** 29–63 (1991).
10. J. Cavanagh, W. J. Fairbrother, A. G. P. III, and N. J. Skelton, "Protein NMR Spectroscopy: Principles and Practice," Academic Press, San Diego (1996).
11. T. A. Cross and S. J. Opella, Solid-state NMR structural studies of peptides and proteins in membranes, *Curr. Opinions Struct. Biol.* **4,** 574–581 (1994).
12. M. M. Maricq and J. S. Waugh, NMR in rotating solids, *J. Chem. Phys.* **70,** 3300–3316 (1979).
13. S. K. Straus, T. Bremi, and R. R. Ernst, Resolution enhancement by homonuclear J decoupling in solid-state MAS NMR, *Chem. Phys. Lett.* **262,** 709–715 (1996).
14. B. A. Tounge, A. K. Mehta, and K. W. Zilm, High field CP MAS of fully ^{13}C labeled polycrystalline compounds, *38th Experimental NMR Conference,* Orlando, 1997.
15. R. G. Griffin, P. R. Costa, J. D. Gross, M. Hatcher, M. Hong, J. Hu, L. Mueller, C. M. Rienstra, S. Fesik, and J. Herzfeld, Structural studies with solid-state NMR: Assignments, distances and torsion angles, *Experimental NMR Conference,* Asilomar, CA, 1998.
16. S. Kiihne, M. A. Mehta, J. A. Stringer, D. M. Gregory, J. C. Shiels, and G. P. Drobny, Distance measurements by dipolar recoupling two-dimensional solid-state NMR, *J. Phys. Chem. A* **102,** 2274–2282 (1998).
17. S. Vijay-Kumar, C. E. Bugg, and W. J. Cook, Structure of ubiquitin refined at 1.8 Å resolution., *J. Mol. Biol.* **194,** 531–544 (1987).
18. D. L. Stefano and A. J. Wand, Two-dimensional 1H NMR study of human ubiquitin: A main chain directed assignment and structure analysis, *Biochemistry* **26,** 7272–7281 (1987).
19. P. L. Weber, S. C. Brown, and L. Mueller, Sequential proton NMR assignments and secondary structure identification of human ubiquitin, *Biochemistry* **26,** 7282–7290 (1987).
20. A. C. Wang and A. Bax, Determination of the backbone dihedral angles f in human ubiquitin from reparameterized empirical Karplus equations, *J. Am. Chem. Soc.* **118,** 2483–2494 (1996).
21. M. Ernst and R. R. Ernst, Heteronuclear dipolar cross-correlated cross relaxation for the investigation of side-chain motions, *J. Magn. Reson.* **110,** 202–213 (1994).
22. D. M. LeMaster and D. M. Kushlan, Dynamical mapping of *E. coli*

thioredoxin via 13C NMR relaxation analysis, *J. Am. Chem. Soc.* **118,** 9255–9264 (1996).

23. A. L. Lee, J. L. Urbauer, and A. J. Wand, Improved labeling strategy for ^{13}C relaxation measurements of methyl groups in proteins, *J. Biomol. NMR* **9,** 437–440 (1997).

24. M. Hong, J. D. Gross, and R. G. Griffin, Site-resolved determination of peptide torsion angle phi from the relative orientations of backbone N–H and C–H bonds by solid-state NMR, *J. Phys. Chem. B* **101,** 5869–5874 (1997).

25. A. L. Lehninger, D. L. Nelson, and M. M. Cox, "Principles of Biochemistry," Worth Publishers, New York (1993).

26. L. Stryer, "Biochemistry," W.H. Freeman, New York (1995).

27. A. C. Wang, S. Grzesiek, R. Tschudin, P. J. Lodi, and A. Bax, Sequential backbone assignment of isotopically enriched proteins in D2O by deuterium-decoupled HA(CA)N and HA(CACO)N, *J. Biomol. NMR* **5,** 376–382 (1995).

28. P. R. Costa, J. D. Gross, M. Hong, and R. G. Griffin, Solid-State NMR Measurement of ψ in Peptides: A NCCN 2Q-Heteronuclear Local Field Experiment, *Chem. Phys. Lett.* **280,** 95–103 (1997).

29. X. Feng, M. Eden, A. Brinkmann, H. Luthman, L. Eriksson, A. Graslund, O. N. Antzutkin, and M. H. Levitt, Direct determination of a peptide torsion angle ψ by double-quantum solid-state NMR, *J. Am. Chem. Soc.* **119,** 12006–12007 (1997).

30. Y. Ishii, T. Terao, and M. Kainosho, Relayed anisotropy correlation NMR: Determination of dihedral angles in solids, *Chem. Phys. Lett.* **256,** 133–140 (1996).

31. T. Fujiwara, T. Shimomura, and H. Akutsu, Multidimensional solid-state nuclear magnetic resonance for correlating anisotropic interactions under magic-angle spinning conditions, *J. Magn. Reson.* **124,** 147–153 (1997).

32. M. Hong and K. Jakes, Selective and extensive ^{13}C labeling of a membrane protein for solid-state NMR investigation, *J. Biomol. NMR* **14,** 71–74.

33. D. C. Muchmore, L. P. McIntosh, C. B. Russell, D. E. Anderson, and F. W. Dahlquist, Expression and nitrogen-^{15}N labeling of proteins for proten and nitrogen-15 nuclear magnetic resonance, *Methods Enzymol.* 45–73 (1989).

34. D. M. LeMaster, Deuteration in protein proton magnetic resonance, *Methods Enzymol.* **177,** 23–73 (1989).

35. D. S. Waugh, Genetic tools for selective labeling of proteins with a-^{15}N-amino acids, *J. Biomol. NMR* **8,** 184–192 (1996).

36. A. J. Wand, J. L. Urbauer, R. P. McEvoy, and R. J. Bieber, Internal dynamics of human ubiquitin revealed by ^{13}C-relaxation studies of randomly fractionally labeled protein, *Biochemistry* **35,** 6116–6125 (1996).

37. A. J. Wand, R. J. Bieber, J. L. Urbauer, R. P. McEvoy, and Z. Gan, Carbon relaxation in randomly fractionally ^{13}C-enriched proteins, *J. Magn. Reson.* **108,** 173–175 (1995).

38. M. T. Zell, B. E. Pudden, D. J. W. Grant, and E. J. Munson, Assignment techniques for understanding polymorphism in crystalline organic compounds with solid-state NMR, *39th Experimental NMR Conference,* Asilomar, CA, 1998.

39. D. Weliky and R. Tycko, Determination of peptide conformations by two-dimensional magic angle spinning NMR exchange spectroscopy with rotor synchronization, *J. Am. Chem. Soc.* **118,** 8487–8488 (1996).

40. X. Feng, P. J. E. Verdegem, Y. K. Lee, D. Sandstrom, M. Eden, P. Bovee-Geurts, W. J. d. Grip, J. Lugtenburg, H. J. M. d. Groot, and M. H. Levitt, Direct determination of a molecular torsion angle in the membrane protein rhodopsin by solid-state NMR, *J. Am. Chem. Soc.* **119,** 6853–6857 (1997).

41. R. Tycko, Prospects for resonance assignments in multidimensional solid-state NMR spectra of uniformly labeled proteins, *J. Biomol. NMR* **22,** 239–251 (1996).

42. M. Hong and R. G. Griffin, Resonance assignment for solid peptides by dipolar-mediated ^{13}C/^{15}N correlation solid-state NMR, *J. Am. Chem. Soc.* **120,** 7113–7114 (1998).

43. S. K. Straus, T. Bremi, and R. R. Ernst, Experiments and strategies for the assignment of fully ^{13}C/^{15}N-labeled polypeptides by solid state NMR, *J. Biomol. NMR* **12,** 39–50 (1998).

44. T. E. Creighton, "Proteins: Structures and Molecular Properties," W.H. Freeman, New York (1993).

45. G. N. Ramachandran and V. Sasisekharan, Conformation of polypeptides and proteins, *Adv. Protein Chem.* **23,** 283–437 (1968).

46. M. Hong, J. D. Gross, C. M. Rienstra, R. G. Griffin, K. K. Kumashiro, and K. Schmidt-Rohr, Coupling amplification in 2D MAS NMR and its application to torsion angle determination in peptides, *J. Magn. Reson.* **129,** 85–92 (1997).

47. G. Wagner and K. Wuthrich, Sequential resonance assignments in protein ^{1}H nuclear magnetic resonance spectra, *J. Mol. Biol.* **155,** 347–366 (1982).

48. M. Baldus and B. H. Meier, Total correlation spectroscopy in the solid state. The use of scalar couplings to determine the through-bond connectivity, *J. Magn. Reson. A* **121,** 65–69 (1996).

49. B. Q. Sun, C. M. Rienstra, P. R. Costa, J. Herzfeld, J. Williamson, and R. G. Griffin, 3D ^{15}N–^{13}C–^{13}C chemical shift correlation spectroscopy in rotating solids, *J. Am. Chem. Soc.* **119,** 8540–8546 (1997).

50. A. Lesage, C. Auger, S. Caldarelli, and L. Emsley, Determination of through-bond carbon–carbon connectivities in solid-state NMR using the INADEQUATE experiment, *J. Am. Chem. Soc.* **119,** 7867–7868 (1997).

51. Z. Gu and S. J. Opella, ^{1}H–^{15}N–^{13}C triple-resonance solid-state NMR experiments for peptides and proteins, *Rocky Mountain Conference on Analytical Chemistry,* Denver, 1998.

52. A. E. McDermott, T. Polenova, G. Montelione, K. Zilm, E. Paulsen, R. Martin, and G. Coker, Multidimensional solids NMR of a uniformly labeled protein, *40th Experimental NMR Conference,* Orlando, 1999.

53. T. Gullion and J. Schaefer, Rotational echo double resonance NMR, *J. Magn. Reson.* **81,** 196–200 (1989).

54. M. Hong, Resonance assignment of ^{13}C/^{15}N labeled proteins by two- and three-dimensional magic-angle-spinning NMR, *J. Biomol. NMR,* in press (1999).

55. P. L. Poole and J. L. Finney, Hydration-induced conformational and flexibility changes in lysozyme at low water content, *Int. J. Biol. Macromol.* **5,** 308–310 (1983).

56. S. D. Kennedy and R. G. Bryant, Structural effects of hydration: Studies of lysozyme by ^{13}C solids NMR, *Biopolymers* **29,** 1801–1806 (1990).

57. R. B. Gregory, M. Gangoda, R. K. Gilpin, and W. Su, The influence of hydration on the conformation of lysozyme by solid-state ^{13}C-NMR spectroscopy, *Biopolymers* **33,** 513–519 (1993).

58. A. Bax and G. A. Morris, Refocused INEPT, *J. Magn. Reson.* **42,** 501 (1981).

59. B. H. Meier, Cross polarization under fast magic-angle spinning: Thermodynamic considerations, *Chem. Phys. Lett.* **188,** 201–207 (1992).

60. S. Hediger, V. H. Meier, and R. R. Ernst, Cross polarization under fast magic angle spinning using amplitude-modulated spin-lock sequences, *Chem. Phys. Lett.* **213,** 627–635 (1993).

61. A. E. Bennett, C. M. Rienstra, M. Auger, K. V. Lakshmi, and R. G.

Griffin, Heteronuclear decoupling in rotating solids, *J. Chem. Phys.* **103,** 6951–6958 (1995).

62. T. Gullion and J. Schaefer, Detection of weak heteronuclear dipolar coupling by rotational-echo double-resonance nuclear magnetic resonance, *in* "Advances in Magnetic Resonance" (W. S. Warren, Ed.), pp. 57–83, Academic Press, San Diego (1989).

63. C. A. Michal and L. W. Jelinski, REDOR 3D: Heteronuclear distance measurements in uniformly labeled and natural abundance solids, *J. Am. Chem. Soc.* **119,** 9059–9060 (1997).

64. W.-K. Rhim, D. D. Elleman, and R. W. Vaughan, Analysis of multiple-pulse NMR in solids, *J. Chem. Phys.* **59,** 3740–3749 (1973).

65. W. T. Dixon, Spinning-sideband-free and spinning-sideband-only NMR spectra in spinning samples, *J. Chem. Phys.* **77,** 1800–1809 (1982).

66. M. G. Munowitz, R. G. Griffin, G. Bodenhausen, and T. H. Huang, Two-dimensional rotational spin-echo NMR in solids: Correlation of chemical shift and dipolar interactions, *J. Am. Chem. Soc.* **103,** 2529–2533 (1981).

67. A. C. Kolbert, D. P. Raleigh, M. H. Levitt, and R. G. Griffin, Two-dimensional spin-echo nuclear magnetic resonance in rotating solids, *J. Chem. Phys.* **90,** 679–689 (1989).

68. J. E. Roberts, G. S. Harbison, M. G. Munowitz, J. Herzfeld, and R. G. Griffin, Measurement of heteronuclear bond distances in polycrystalline solids by solid-state NMR techniques, *J. Am. Chem. Soc.* **109,** 4163–4169 (1987).